

Crack interaction and localization in tunnel linings

M. Nakano & Z. Shi

R&D Center, Nippon Koei Co., Ltd., Tsukuba, Ibaraki, Japan

ABSTRACT: To examine how cracks interact with each other in tunnel linings, the fracture test of a tunnel specimen is studied numerically to obtain the coefficient of interaction, which is derived based on the extended fictitious crack model (EFCM). Under the test conditions, five cracks propagate in five separate tension zones from the initial notches that are preset in the numerical model. Unlike the bending tests of beams where all the cracks originate from the same tension side, crack interaction and localization in tunnel linings exhibit characteristics that are unique to structures with several tension zones when subjected to loading.

1 INTRODUCTION

In studying cracking behaviors in various concrete structures, it has been noted that crack interactions in beams and in tunnel linings show fundamental differences (Shi 2009). For a beam under bending, cracks emerge from the same tension side and the crack interaction facilitates crack propagation, as

shown in Figure 1(a). On the other hand, when multiple tension zones coexist in a deformed structural member as illustrated in Figure 1(b), cracks from different tension zones interact and hinder the growth of each other. This diminishing effect of crack interaction in tunnel linings is the focus of the present study.

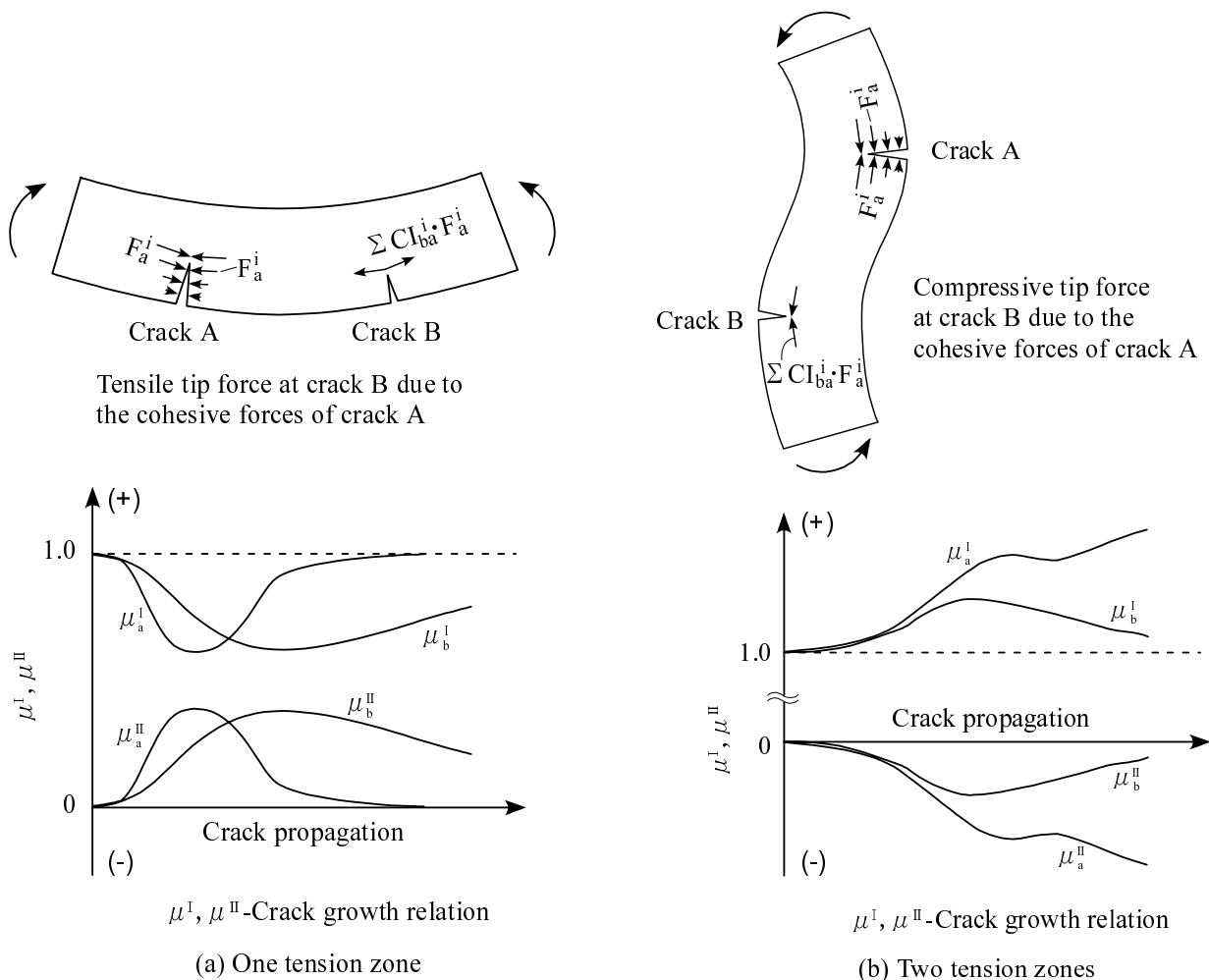


Figure 1. Characteristics of crack interactions with (a) one and (b) two tension zones.

2 COEFFICIENT OF INTERACTION

In the discrete approach that allows the interaction of multiple cracks to be studied most straightforwardly, an explicit mathematical formulation of the crack interaction is possible (Shi et al. 2004). Such an approach enables crack interaction to be quantified and various cracking behaviors to be studied based on the nature and the intensity of the crack interactions involved. In order to derive the coefficient of interaction, the crack equations for a three-crack problem are presented below, which are then used to define the coefficient of interaction.

2.1 Crack equations

Figure 2 illustrates three cracks of the mode-I type, cracks A, B and C. If crack A is assumed to be the only active crack, the tensile force at its tip must reach the nodal force limit Q_{la} , as shown in Figure 2(e),

$$Q_{la} = CR_a \cdot P_a + \sum_{i=1}^{N1} CI_{aa}^i F_a^i + \sum_{j=1}^{N2} CI_{ab}^j F_b^{*j} + \sum_{l=1}^{N3} CI_{ac}^l F_c^{*l} \quad (1)$$

where $N1$, $N2$ and $N3$ are the number of nodes inside the three fictitious cracks, respectively. Here, CR_a , CI_{aa}^i , CI_{ab}^j and CI_{ac}^l represent the tensile forces at the tip of crack A due to a unit external load, and a pair of unit cohesive forces at the i -th node of crack A, the j -th node of crack B, and the l -th node of crack C, respectively. These coefficients are determined by FE calculations of the models in Figure 2(a-d). Note that P_a is the load required to propagate crack A, while crack B and crack C remain inactive.

The CODs along the three fictitious cracks are given by

$$W_a^i = BK_a^i \cdot P_a + \sum_{k=1}^{N1} AK_{aa}^{ik} F_a^k + \sum_{j=1}^{N2} AK_{ab}^{ij} F_b^{*j} + \sum_{l=1}^{N3} AK_{ac}^{il} F_c^{*l} \quad (2)$$

$$W_b^{*j} = BK_b^j \cdot P_a + \sum_{i=1}^{N1} AK_{ba}^{ji} F_a^i + \sum_{k=1}^{N2} AK_{bb}^{jk} F_b^{*k} + \sum_{l=1}^{N3} AK_{bc}^{jl} F_c^{*l} \quad (3)$$

$$W_c^{*l} = BK_c^l \cdot P_a + \sum_{i=1}^{N1} AK_{ca}^{li} F_a^i + \sum_{j=1}^{N2} AK_{cb}^{lj} F_b^{*j} + \sum_{k=1}^{N3} AK_{cc}^{lk} F_c^{*k} \quad (4)$$

where $i = 1, \dots, N1$; $j = 1, \dots, N2$; $l = 1, \dots, N3$. Here, BK_a^i at crack A, BK_b^j at crack B, and BK_c^l at crack C are the compliances at nodes i , j , and l , respectively, due to the external load. The influence coefficients AK_{aa}^{ik} , AK_{ab}^{ij} and AK_{ac}^{il} are the displacements at the i -th node of crack A due to a pair of unit cohesive forces at the k -th node of crack A, the j -th node of crack B, and the l -th node of crack C, respectively. Similarly, the influence coefficients AK_{ba}^{ji} , AK_{bb}^{jk} and AK_{bc}^{jl} represent the displacements at the j -th

node of crack B, and AK_{ca}^{li} , AK_{cb}^{lj} and AK_{cc}^{lk} are the displacements at the l -th node of crack C, respectively due to a pair of unit cohesive forces at the corresponding locations. FE models to compute these coefficients are given in Figure 2(a-d).

Imposing the tension-softening law of concrete along each fictitious crack leads to

$$F_a^i = f(W_a^i) \quad (5)$$

$$F_b^{*j} = f(W_b^{*j}) \quad (6)$$

$$F_c^{*l} = f(W_c^{*l}) \quad (7)$$

Equations (1) to (7) form the crack equations required to propagate crack A. With the number of equations ($2N1 + 2N2 + 2N3 + 1$) matching the number of unknowns ($2N1 + 2N2 + 2N3 + 1$), the problem can be solved uniquely, since these equations are linearly independent. Similarly, the crack equations for propagating crack B or crack C can be obtained.

By solving the three sets of crack equations, the true cracking mode for the next load increment is determined based on the minimum load criterion, and the stress and displacement fields are calculated accordingly. This process is repeated until structural failure.

2.2 Coefficient of interaction and principal tip force coefficient

Equation (1) represents the condition for crack propagation. As seen, the tip force of an active crack is caused by the external loads and its own cohesive forces, and those of the neighboring cracks as well. Obviously, the latter represents the crack interaction. Accordingly, the nodal force components at the tip of an active crack are divided into two parts: the principal tip force (PTF) Q_a^I , Q_b^I and Q_c^I given by

$$Q_a^I = CR_a \cdot P_a + \sum_{i=1}^{N1} CI_{aa}^i F_a^i \quad (8)$$

$$Q_b^I = CR_b \cdot P_b + \sum_{j=1}^{N2} CI_{bb}^j F_b^j \quad (9)$$

$$Q_c^I = CR_c \cdot P_c + \sum_{l=1}^{N3} CI_{cc}^l F_c^l \quad (10)$$

and the secondary tip force (STF) Q_a^{II} , Q_b^{II} and Q_c^{II} , given by

$$Q_a^I = \sum_{j=1}^{N2} CI_{ab}^j F_b^{*j} + \sum_{l=1}^{N3} CI_{ac}^l F_c^{*l} \quad (11)$$

$$Q_b^I = \sum_{i=1}^{N1} CI_{ba}^i F_a^{*i} + \sum_{l=1}^{N3} CI_{bc}^l F_c^{*l} \quad (12)$$

$$Q_c^I = \sum_{i=1}^{N1} CI_{ca}^i F_a^{*i} + \sum_{j=1}^{N2} CI_{cb}^j F_b^{*j} \quad (13)$$

where

$$Q_{la} = Q_a^I + Q_a^{II} \quad (14)$$

$$Q_{lb} = Q_b^I + Q_b^{II} \quad (15)$$

$$Q_{lc} = Q_c^I + Q_c^{II} \quad (16)$$

force. Hence, the interactions of the neighboring cracks may facilitate or hinder the propagation of the active crack, depending on whether the STF is tensile or compressive. To introduce the coefficient of interaction and the PTF coefficient, the PTF and the STF are now divided by the critical tip force, and the resulting non-dimensionalized coefficients μ_a^I , μ_b^I and μ_c^I for the PTF, and μ_a^{II} , μ_b^{II} and μ_c^{II} for the STF, are denoted by

$$\mu_a^I = \frac{Q_a^I}{Q_{la}} \quad (17)$$

$$\mu_b^I = \frac{Q_b^I}{Q_{lb}} \quad (18)$$

$$\mu_c^I = \frac{Q_c^I}{Q_{lc}} \quad (19)$$

$$\mu_a^{II} = \frac{Q_a^{II}}{Q_{la}} \quad (20)$$

Depending on the specific configuration of the problem and the relative locations of the neighboring cracks to the active crack, the resultant of the STF components can either be a tensile force or a compressive

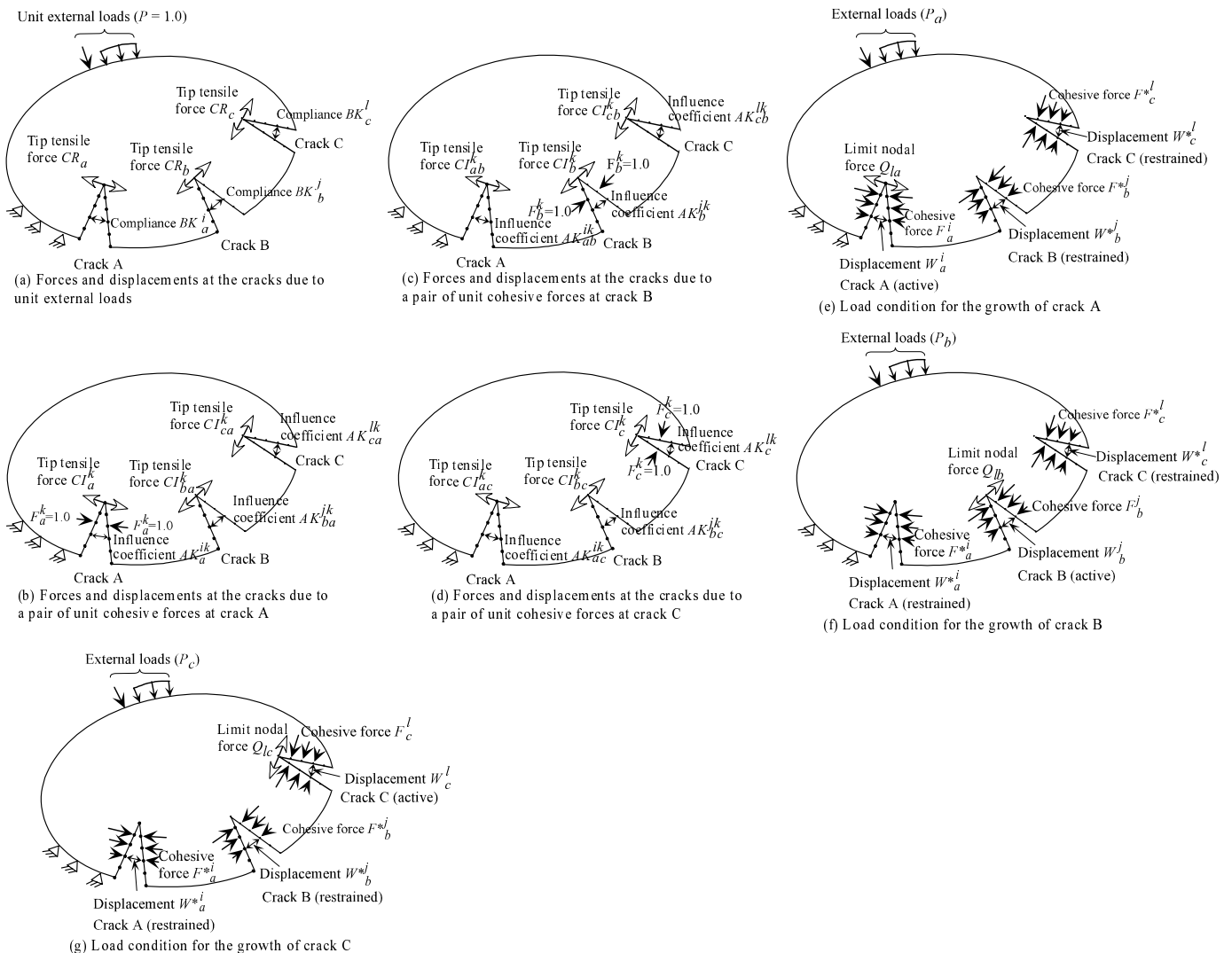


Figure 2. Crack-tip-controlled modeling of three discrete cracks.

$$\mu_b^{II} = \frac{Q_b^{II}}{Q_{lb}} \quad (21)$$

$$\mu_c^{II} = \frac{Q_c^{II}}{Q_{lc}} \quad (22)$$

where

$$\mu_a^I + \mu_a^{II} = 1 \quad (23)$$

$$\mu_b^I + \mu_b^{II} = 1 \quad (24)$$

$$\mu_c^I + \mu_c^{II} = 1 \quad (25)$$

Here, μ_a^{II} , μ_b^{II} and μ_c^{II} are termed the coefficients of interaction, and μ_a^I , μ_b^I and μ_c^I are called the PTF coefficients. Based on the previous analysis, it is known that while μ_a^I , μ_b^I and μ_c^I are always positive, μ_a^{II} , μ_b^{II} and μ_c^{II} can be either positive or negative.

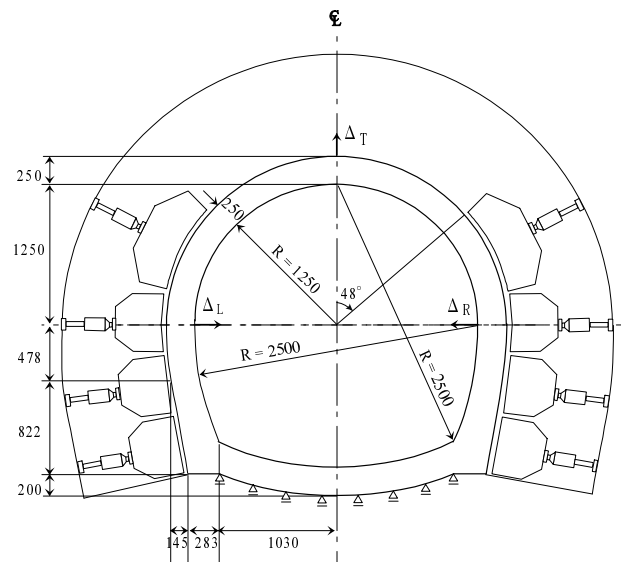
3 FRACTURE TEST ON TUNNEL LINING SPECIMEN

The fracture test of a real-size concrete lining specimen of a waterway tunnel is shown in Figure 3 (Abo et al. 2000). The test was carried out to investigate the cracking behavior and fracture process of a tunnel lining with void formation above the ceiling area. Although no measurements of the CMODs were taken during the test, the crack trajectories were carefully recorded, as shown in Figure 4. As seen, five cracks propagated in the test specimen before the tunnel collapsed under compression. The most active crack occurred in the right wall, which was followed by two progressive cracks in the bottom plate from outside. The crack in the left wall and the crack in the ceiling area from outside were small and less ac-

tive. Upon reaching the peak load the tunnel specimen failed in a brittle fashion, as indicated in the load-displacement relations. It was reported that during the experiment a certain degree of eccentric loading occurred, generating a higher pressure-load on the right wall. The material properties of the test specimen are summarized in Table 1.

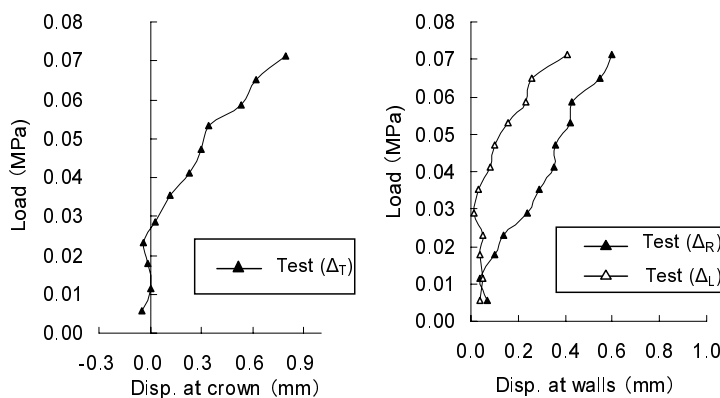
4 NUMERICAL STUDIES

Crack analysis is carried out using a full FE model with five initial notches assumed based on the exact crack locations observed during the test, as shown in Figure 5. Since the ratio of the actual eccentric loads that occurred during the test was unknown, the uniformly distributed loads on the two sidewalls are assumed to be equal, but the vertical supports under the right portion of the bottom plate are removed to simulate the un-symmetric boundary conditions of the test.



Dimensions in mm

Figure 3. Fracture test on tunnel specimen.



(a) Load-displacement relation

(b) Crack propagation chart

Figure 4. Results of fracture test on tunnel specimen.

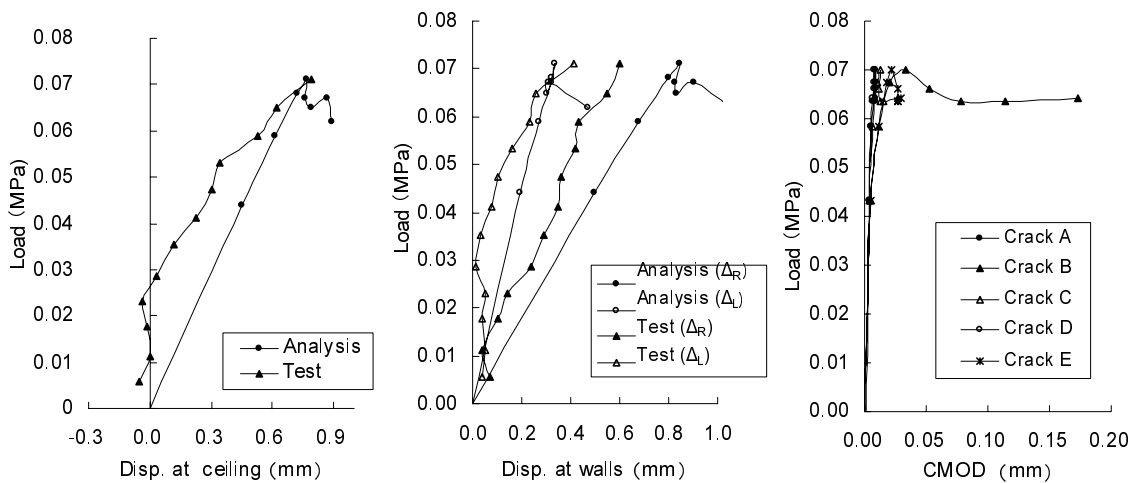
Table 1. Material properties of tunnel specimen.

E (GPa)	ν	F_c (Mpa)	F_t (MPa)	G_F (N/mm)
20..	0.20	20.00	2.00	0.10

From the crack propagation charts and the load-CMOD relations, crack B is shown to be the dominant crack, and its simultaneous propagation with crack E in the first five steps illustrates the vulnerability of the sidewalls to cracking. The growth of crack C in the bottom plate is slow initially. Crack A and crack D are much less active. Upon reaching the peak load, the active growth of crack E stops and it becomes a non-propagating crack in the postpeak regions. On the other hand, though crack C is less active in the prepeak region, it becomes a fast propagating crack from the fourteenth step in the postpeak regions. The belated rigorous growth behavior of crack C is closely related to the progres-

sive opening of crack B in the sidewall, which leads to the large structural deformation in the tunnel specimen that in turn causes a substantial bending moment to form at the right portion of the bottom plate to propagate crack C. In general, the numerically obtained cracking behaviors represent closely the crack propagation patterns of the test, except for crack D. The recorded large crack at notch D is not reproduced by the numerical analysis, probably due to the inaccuracy in the assumed boundary conditions for the actual situation.

Perhaps the most interesting feature of the crack interaction in the tunnel specimen is represented by the negative coefficient of interaction, as shown in Figure 6. With several tension zones coexisting in the tunnel lining, the cohesive forces at one crack induce a compressive tip force component at another crack in a different tension zone, which tends to close that crack. Apparently, this is the effect of reversing or



(a) Load-displacement relation

(b) Load-CMOD relation

(c)

(d)

Figure 5. Results of crack analysis by full FE model.

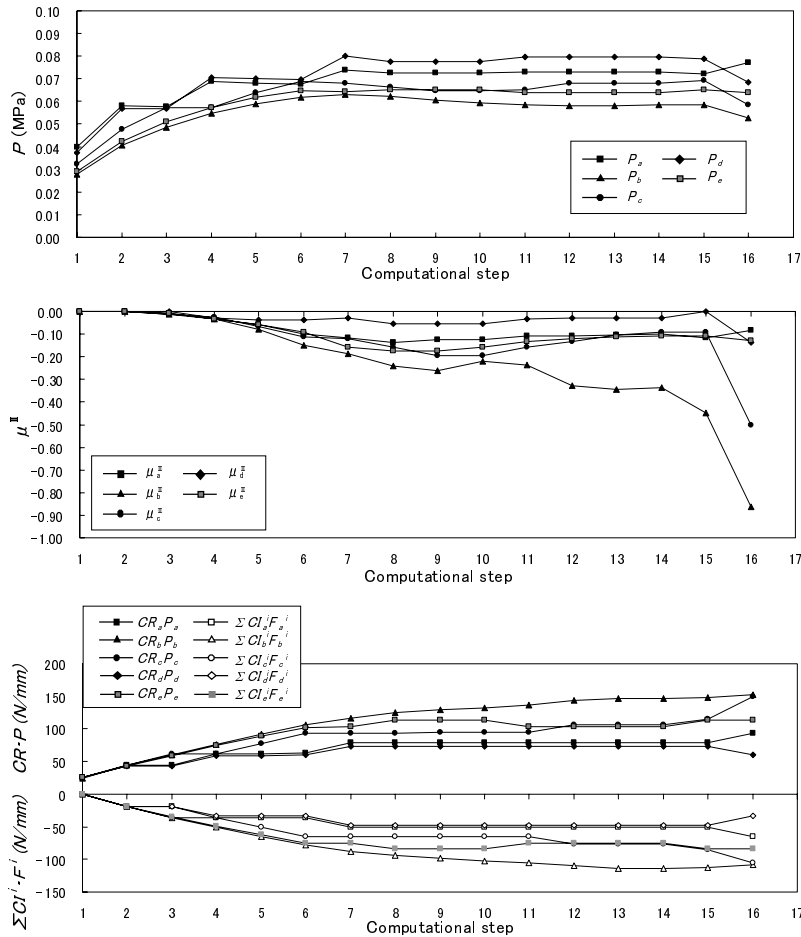


Figure 6. External loads, coefficients of interaction and principal tip-force components for each assumed active crack.

resisting the structural deformation by the cohesive forces of a crack in any tension zones. Therefore, the crack interactions in these situations actually represent the resistance to the growth of a crack. This leads to an interesting phenomenon: the more active a crack becomes, the stronger resistance it encounters. This fact can be verified by the large interaction coefficients of crack B in Figure 6. Note that as the coefficient of interaction becomes negative, the PTF coefficient must be greater than one, according to Equations (23) to (25). The stress concentration at crack B gradually becomes evident as the crack propagates in the postpeak regions, though with a much-reduced magnitude as compared to the scale of the stress concentration observed at a propagating crack in the beam problems.

5 CONCLUSIONS

For structures with several tension zones, cracks in different tension zones interact not through the same tension field but through the general structural deformation that leads to the formation of these tension zones, as shown in Figure 1. As the cohesive forces of one crack tend to close that crack and thus resist general structural deformation, a compressive force

is induced at the tip of another crack, which is equivalent to increasing the material resistance to fracture. Hence, the coefficients of interaction become negative, and the magnitudes of these coefficients represent the amount of the increased resistance encountered in propagating these cracks. This increment of resistance is reflected in the PTF coefficients that are greater than one, as shown in Figure 1. Consequently, with multiple tension zones coexisting the more active a crack becomes, the larger structural deformation it causes, which in turn activates more cracks in other tension zones and thus results in more interaction or resistance to the propagation of that active crack.

REFERENCES

- Abo, H., Tanaka, M., & Yoshida, N. (2000). "Development of a maintenance system for waterway tunnels." *Electric Power Civil Engineering*, JEPOC, Tokyo, No. 287, 42-46.
- Shi, Z. (2009). "Crack interaction and localization." *Crack Analysis in Structural Concrete: Theory and Applications*, Elsevier, 119-148.
- Shi, Z., Suzuki, M., & Ohtsu, M. (2004). "Discrete modeling of crack interaction and localization in concrete beams with multiple cracks." *J. Advanced Concrete Technology*, JCI, 2(1), 101-111.